Reversibility of Al/Ti Modified $LiBH_4$

D. Blanchard,*,† Q. Shi,† C. B. Boothroyd,‡ and T. Vegge†

Materials Research Division, Risø National Laboratory for Sustainable Energy, and Center for Electron Nanoscopy, Technical University of Denmark

Received: April 7, 2009; Revised Manuscript Received: June 4, 2009

Lithium borohydride has a high reversible hydrogen storage capacity. For its practical use as an on-board hydrogen storage medium in mobile applications, the temperature and pressure conditions along with the kinetics of the hydrogenation/dehydrogenation cycles have to be improved. Lithium borohydride can be modified by ball-milling with Al- and/or Ti-containing compounds. In this study, lithium alanate ($LiAlH_4$), is used as an Al source. From careful examination of the ball-milled samples, it appears that $LiBH_4$ remains unchanged during milling. The samples contain ~100 nm diameter Al and/or Al−Ti solid solution (ss) crystallites. When used alone, Ti has a limited effect whereas Al is shown to be active, lowering the temperature of decomposition and increasing the desorption rate and reversibility at moderate temperature and pressure (85 bar, 350 °C). During cycling, AlB_2 is formed in the dehydrogenated state and disappears in the hydrogenated state; its formation increases the stability of the products and thus results in a lower desorption temperature. The Al−Ti (ss) also allows a slow release of hydrogen at very low temperatures (200 °C).

1. Introduction

In the study of high gravimetric hydrogen storage materials, lithium borohydride ($LiBH_4$) is an attractive system for on-board applications. The light weight of its elements added to the number of hydrogen atoms per metal atom, H/M = 2, gives a gravimetric hydrogen capacity of 18.5 wt % for a volumetric density of 121 kg H_2/m^3. However, $LiBH_4$ is thermodynamically too stable for the hydrogenation/dehydrogenation cycles to proceed at practical pressures and temperatures.[1] Upon heating to 108−112 °C, $LiBH_4$ undergoes a reversible polymorphic transformation from an orthorhombic (space group *Pnma*) to a hexagonal structure (space group $P6_3mc$)[2] possibly with disordered BH_4 complexes.[3,4] At 275−278 °C $LiBH_4$ melts, and at temperature above 380 °C it decomposes, releasing 80% of its total hydrogen content. At 483−492 °C, a thermal analysis shows an unexplained endothermic effect which coincides with the liberation of 50% of its remaining hydrogen content.[5] The complete dehydrogenation reaction can be simplified as follows[6−8] without mentioning the possible formation of the intermediate $Li_2B_{12}H_{12}$ species:[9−11]

$$LiBH_4 \rightarrow LiH + B + \frac{3}{2}H_2 \rightarrow Li + B + 2H_2 \quad (1)$$

The first step liberates 13.8 wt % H_2 at temperature from 380 up to 492 °C, and the second step liberates 4.7 wt % at too high temperature to be considered for onboard hydrogen storage.

A possible way to destabilize complex hydrides and/or catalyze the hydrogenation/dehydrogenation reactions and further tune their thermodynamic and kinetic characteristics is the use of selected additives. These additives are usually mixed with the hydrides by high-energy milling. Several additives have been found to destabilize $LiBH_4$ and make the hydrogenation/dehydrogenation possible at rather moderate pressures and temperatures. In 1980, Muller et al.[12] used aluminum as an additive to improve the hydrogenation/dehydrogenation cycle of $LiBH_4$. More recently, with the growing interest in complex hydrides, several studies have been conducted. Züttel et al.[13] lowered the temperature of decomposition by using SiO_2 and achieved the reversibility (result not shown). Vajo et al.[14] used $MgH_2 + TiCl_3$ as additives and achieved reversibility with formation of metallic Mg or MgB_2 in the dehydrogenated state depending on the applied pressure. Orimo et al.[15] used Mg alone as an additive. They proved that pure $LiBH_4$ is reversible at 350 bar and 600 °C but did not give any data for the mixed system. Yu et al.,[16] following Vajo et al.,[14] used MgH_2 alone and formed both MgB_2 and Li−Mg phases during thermal decomposition. They achieved reversibility at 400 °C under 100 bar of H_2. The destabilization of lithium borohydride using Al or MgH_2 was also predicted by thermodynamic calculation in ref 17 and experimentally confirmed for Al.[18,19] This nonexhaustive list of the first work on lithium borohydride as a material for hydrogen storage shows that there are many ways of achieving reversible storage at less extreme conditions with the use of selected additives.

In the present paper we discuss the ability of Al and $TiCl_3$ additives to moderate the conditions for hydrogenation and dehydrogenation of $LiBH_4$. After ball-milling of $LiBH_4$ with the additives, the compounds obtained were carefully studied in order to understand the reactions taking place during ball-milling. For some selected systems, the evolution of reversible storage capacity and the composition were studied. Powder X-ray diffraction (PXD), transmission electron microscopy (TEM), and thermal desorption spectroscopy (TDS) were used to analyze the systems (hydride + additives).

2. Experimental Section

All the commercial chemical compounds were used as received as powders without further purification. $LiBH_4$ (no.

* To whom correspondence should be addressed. E-mail: didier.blanchard@risoe.dk.
† Risø National Laboratory for Sustainable Energy.
‡ Center for Electron Nanoscopy.

10.1021/jp9031892 CCC: $40.75
Published on Web 07/01/2009

TABLE 1: List of the Modified $LiBH_4$-Based Materials[a]

samples	composition	temperature (°C)	H_2 wt %
a	as received $LiBH_4$	480	12.7
b	$2LiBH_4 + LiAlH_4 + 4$ mol % $TiCl_3$	436	6
c	$LiBH_4 + LiAlH_4 + 4$ mol % $TiCl_3$	417	6.2
d	$LiBH_4 + 3LiAlH_4 + 4$ mol % $TiCl_3$	390	7
e	$LiBH_4 + 3LiAlH_4$	460	8.9
f	$LiBH_4 + 3(LiH + Al) + 2$ mol % $TiCl_3$	400	2.6
g	$3LiBH_4 + LiH + Al + 2$ mol % $TiCl_3$	500	2.6
h	$LiBH_4 + 10$ mol % $(LiCl + 3Al + Ti)$	490	7.2
I	$LiBH_4 + 2$ mol % $TiCl_3$	480	11.1
j	$LiBH_4 + 3(LiH + Al)$	400	2.4

[a] The temperatures refer to the end of the desorption process. In samples f, g, and j, LiH + Al was obtained from thermal decomposition of $LiAlH_4$ up to 210°C (see eqs 2 and 3). In sample h, LiCl + 3Al + Ti was obtained from a ball-milled stoichiometric mixture of $3LiAlH_4 + TiCl_3$. H_2 wt % is the weight percentage of hydrogen released.

62460, 95.0% gas-volumetric), $TiCl_3$ (99.999%), and $LiAlH_4$ (95%, LiCl present as an impurity) were purchased from Sigma-Aldrich (Fluka and Riedel Co.).

All sample storage and handling was performed in an inert gas (Ar) glovebox. A high-energy mixer mill from Glen Creston Ltd., was employed to mix and catalyze the samples under an argon atmosphere at 200 rpm. A Teflon O-ring sealed the stainless steel ball-mill vial and five tungsten carbide balls (total weight 31 g) were used. Each time, 1−2 g of sample was prepared with 30 min of ball-milling, the ball to powder weight ratio being 30:1 or 15:1.

Thermal desorption spectra of hydrogen were measured in a Sievert's type system under 1 bar of He. The Sievert's reactor was heated at a selected heating ramp (0.5 °C/min for most of the samples presented here) in a Carbolite furnace. About 0.25−1 g of sample was used in each experiment. A valve on the reactor prevented the powder from being exposed to air during transportation from the glovebox to the TDS. The minimum operation time between the end of the milling and the start of the TDS was 20 min.

PXD spectra were recorded on two Bragg−Brantano diffractometers, a STOE (40 kV, 30 mA, Cu radiation $K_\alpha = 1.542$ Å), and a BRUKER D8 (40 kV, 40 mA, Cu radiation $K_\alpha = 1.542$ Å). To avoid contact with air or moisture, specially designed airtight PXD sample holders were used. The STOE sample holder contains a piece of Si to allow the sample holder height to be adjusted in the X-ray beam. Therefore, STOE PXD patterns contain Si diffraction peaks at $2\theta = 28.44°$, 47.30°, and 56.12°. For the Bruker D8 sample holder a polyethylene film was used to protect the sample from air contamination. The film gives rise to a broad peak at around 22° in 2θ, together with one peak from the sample holder itself at 43.5°. These peaks were excluded from the patterns during the Rietveld refinements. The refinements were performed using Rietica software.[20] The structural data for $LiBH_4$ were taken from ref 21.

TEM imaging was performed on a Tecnai T20 at the Center for Electron Nanoscopy, DTU. To avoid reaction of the sample with oxygen and air moisture, N_2 gas was flowed over the sample holder during loading into the TEM.

3. Results and Discussion

3.1. First Dehydrogenation. Here we present and discuss the TDS data for the first dehydrogenation of the ball-milled samples. Table 1 displays the composition of the samples, the temperatures at the end of the desorption, and the final H_2 wt %. These results are extracted from the TDS curves shown in Figures 1 and 2. The release of hydrogen at very low temperature (<100 °C) (Figure 1) is due to the presence of $LiAlH_4$. Lithium alanate is the first to release hydrogen during TDS. Its decomposition temperature is lower than that of $LiBH_4$. The first two decomposition steps (eqs 2 and 3[21]), are visible on the plots for samples b, c, d, and e) at about 60 and 100 °C. These reactions were confirmed for sample c by PXD (Figure 3) and are the same for the other samples. The reaction in eq 4 occurs at rather high temperature (650 °C[21]) and does not occur with the condition of this study.

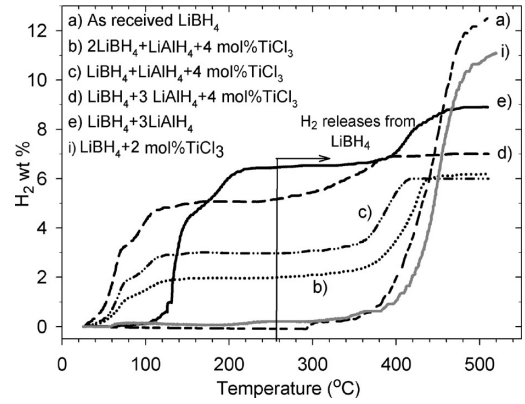

Figure 1. TDS plots of the first dehydrogenation for the as-milled samples a−e and i.

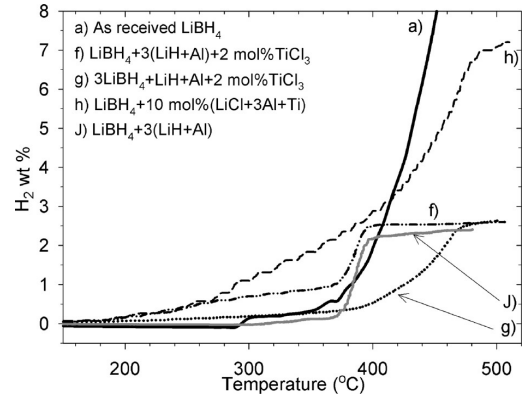

Figure 2. TDS plots of the first dehydrogenation for the as-milled samples f−h.

At room temperature, after milling, sample c was composed of $LiBH_4$, $LiAlH_4$, Al, and LiCl, no Ti was detected, Figure 3-I. When the sample was heated to 80 °C, $LiAlH_4$ decomposed and formed Li_3AlH_6, Figure 3-II. Finally, when the sample was heated to 150 °C, Li_3AlH_6 vanished while $LiBH_4$ remained as observed in the sample at room temperature, Figure 3-III.

$$LiAlH_4 \rightarrow Li_3AlH_6 + Al + H_2 \quad (2)$$

$$Li_3AlH_6 \rightarrow 3LiH + Al + H_2 \quad (3)$$

$$LiH + Al \rightarrow LiAl + H_2 \quad (4)$$

For all the samples containing $LiAlH_4$, the decomposition follows the same route. The lithium alanate is decomposed, and then the lithium borohydride starts to release hydrogen. While the temperatures for lithium alanate to decompose are the same for all the samples (except e), the temperatures for lithium

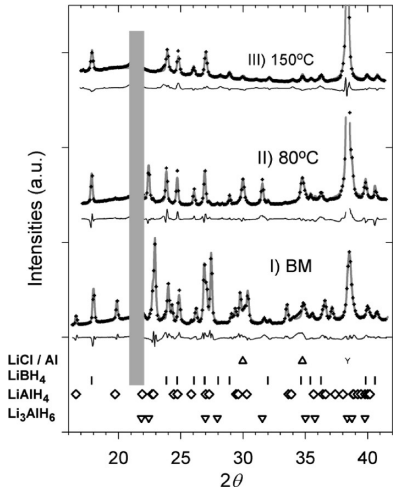

Figure 3. BRUKER PXD patterns for sample c at different stages of decomposition. The sample was heated and cooled to room temperature. Positions of (Δ) LiCl, (Y) Al, (|) $LiBH_4$, (◇) $LiAlH_4$, and (▽) Li_3AlH_6 Bragg peaks. The dots are the experimental points, the gray lines are the refined patterns, and the lines under each pattern are the difference between the experimental and the refined patterns. The gray rectangles are the regions excluded from the refinement (peaks due to the plastic film).

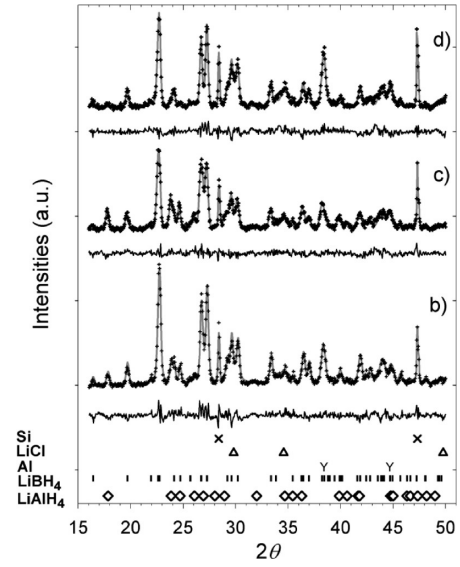

Figure 4. STOE PXD patterns of samples b, c, and d. The dots are the experimental points, the lines are the refined patterns, and the lines under each pattern are the differences between the experimental and the refined patterns. Positions of (×) Si, (Δ) LiCl, (Y) Al, (|) $LiBH_4$, and (◇) $LiAlH_4$ Bragg peaks.

borohydride are inversely proportional to the Alanate content (samples b, c, and d). For sample e, with no $TiCl_3$, the temperature for $LiBH_4$ decomposition is the same as the decomposition temperature of pure $LiBH_4$.

For sample i, $LiBH_4$ + 2 mol % $TiCl_3$, the curve is very close to the curve for pure $LiBH_4$ (see Figure 2) and there is no decrease in the temperature of decomposition.

From this first batch of samples it clearly appears that a synergistic effect exists between the two additives, $TiCl_3$ and $LiAlH_4$, acting to decrease the decomposition temperature of $LiBH_4$.

To further explore and understand these results, the following samples were prepared. In samples f, g, and i, $LiAlH_4$ was first thermally decomposed into LiH+Al (eqs 2 and 3[22]) and then ball-milled with $LiBH_4$. In sample h, a stoichiometric mixture of $3LiAlH_4$ + $TiCl_3$, was first ball-milled for 30 min at 200 rpm then ball-milled with $LiBH_4$ in the ratio of 10 mol %.

The TDS curves for these samples are shown in Figure 2. It is interesting to compare the curves for samples f, j, and h. Samples f and j decompose at the same temperature and exhibit the same fast release of hydrogen. Nevertheless, for sample f a slow release of hydrogen occurs at the rather low temperature of ~150 °C. This slow release does not exist for sample j but is present for sample h. Sample h, in contrast, does not show this rapid release in its decomposition.

It is possible to interpret these results as a separate effect from the two additives, Al and Ti. Ti may give the slow evolution of hydrogen at low temperatures, while Al may help in the fast decomposition. However, from the TDS curves of sample i it is clear that $TiCl_3$ alone has a limited effect. If Al works alone, Ti needs Al to promote its effect! To further investigate this observation, PXD and TEM imaging were conducted on the as-milled sample. The results are shown in the following sections.

3.2. Examination of the Sample after Ball-Milling. ***3.2.1. $LiBH_4$ Mixed with $LiAlH_4$ and $TiCl_3$.*** In Figure 4, the diffraction patterns collected from samples b, c, and d are plotted. No $TiCl_3$ is observed in any of the samples, and the only phases that are detectable, within the limit of the technique and of our equipment, are $LiBH_4$, $LiAlH_4$, LiCl, and Al. The phase compositions of the samples, obtained from quantitative phase analysis, are presented in Table 2. The results are in good agreement with the following reaction occurring during milling:

TABLE 2: Composition (mol %) Obtained from Quantitative Phase Analysis (QPA) on the Refined Diffraction Patterns of Samples b, c, and d

samples	$LiBH_4$	$LiAlH_4$	Al	LiCl
b	55 (59)[a]	20 (19)	12 (10.7)	13 (10.7)
c	50 (44)	33 (34)	8.5 (10.7)	7.5 (10.7)
d	46 (40)	18 (21)	19 (19)	17 (19)

[a] The numbers in parentheses correspond to the theoretical value calculated from eq 5.

$$LiBH_4 + xLiAlH_4 + yTiCl_3 \xrightarrow{BM} LiBH_4 + (x - 3y)LiAlH_4 + 3yLiCl + 3yAl + yTi + 6yH_2 \quad (5)$$

This reaction describes the reduction of the chloride by the Alanate, leaving $LiBH_4$ apparently unchanged. The reduction reaction has been well studied for both sodium and lithium alanate when ball-milled with chlorides.[23−25] It achieves a fine dispersion of Ti and Al on the grain surfaces. It is known that for sodium alanate ball-milled with titanium chloride, a solid solution of Ti and Al gradually forms.[23,26] In our case, due to the limited resolution of the diffractometer and the low molar percentage of Ti, it is not possible to detect such a solid solution. Furthermore, some phases present as traces or in the amorphous state may also exist.

To investigate the microstructure of the samples, sample d ($LiBH_4$ + $3LiAlH_4$ + 4 mol % $TiCl_3$) was imaged using TEM. Figure 5a shows a dark-field image of a typical particle whose overall size is around 2 μm across. It is supported on a holey carbon film, some of which is visible at the top. It can be seen that the particle has a porous structure. The bright particles with diameter ≤100 nm are those of individual crystalline grains that are diffracting strongly into the objective aperture. Figure 5b

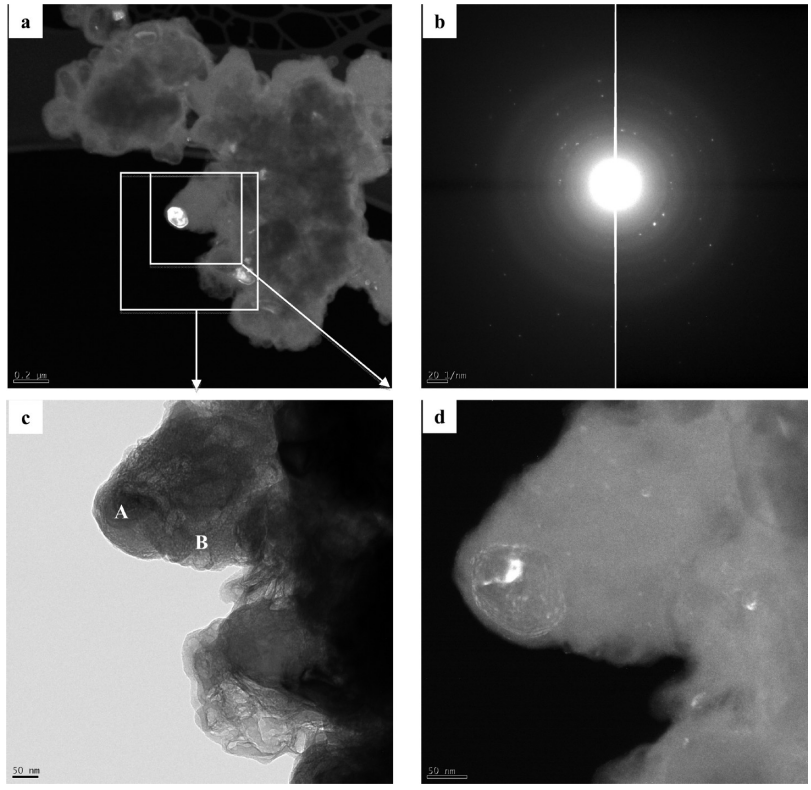

Figure 5. TEM images of sample d, $LiBH_4 + 3LiAlH_4 + 4$ mol % TiCl3. (a) Dark-field image of an agglomerated particle using an Al reflection. (b) Electron diffraction pattern from the region shown in a. (c) Under-focus bright-field image showing voids. (d) Dark-field image showing weakly diffracting Al particle plus smaller crystals.

shows a diffraction pattern from the same region as Figure 5a. The crystalline particles give rise to the sharp spots while the diffuse rings are from amorphous material. There are also some faint rings indicating the presence of much finer grains, some of which can be seen in Figure 5a. Figure 5c shows a slightly under focus bright-field image of an area shown in Figure 5a. Imaging underfocus causes Fresnel fringes to appear at edges enhancing the contrast in voids. We can thus see that the amorphous material in this particle is very porous. Figure 5d is an enlargement of the region surrounding the bright crystalline particle in Figure 5a. The particle has been tilted to a weakly diffracting condition and can be seen to consist of two grains. Also visible are some of the smaller crystalline particles with diameters around 10 nm.

An EDX spectrum from the bright crystal in figure 5a (position A in Figure 5c) showed that it contained mostly Al with a little O and traces of Ti and Cl. In the porous amorphous region next to this particle (position B), an EDX showed the presence of Al, some O, a little Cl, but no Ti. EDX is only able to detect elements with $Z = 6$ (C) or above, meaning that neither Li, B, nor H is detectable.

EELS confirms that the bright crystal (position A) is Al with a strong, sharp plasmon peak at 15 eV plus an Al L edge at 74 eV. Only a small oxygen edge was visible. The porous amorphous region (position B) had a boron edge in addition to Al and O edges. Li was not seen in either area, but its edge overlaps with the plasmon peaks and is thus difficult to see at low concentrations. H is not detectable as its edge is at too low an energy.

TEM thus shows that sample d contains crystalline grains of Al of diameter $\leq$100 nm in a porous amorphous matrix containing Al, B, Cl, and O. Some nanocrystalline grains of diameter $\sim$10 nm are also present.

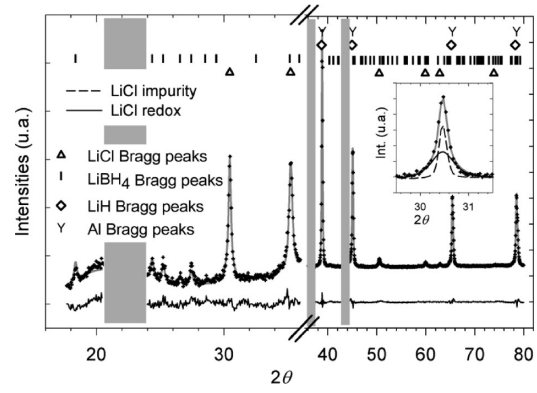

Figure 6. BRUKER PXD pattern of sample f. The dots are the experimental points; the gray line is the refined pattern. The black line under the pattern is the difference between the experimental and the refined pattern. The gray rectangles are the regions excluded from the refinement (peaks due to the plastic film and the sample holder). The plot has been divided in two plots with different scales in order to show the low intensity peak due to $LiBH_4$ (left side of the plot). The insert shows the LiCl (111) peak fitted with two LiCl phases, (—) LiCl from the reduction reaction, (— — —) LiCl from $LiAlH_4$.

3.2.2. $LiBH_4$ Mixed with LiH + Al and $TiCl_3$. In Figure 6, a PXD pattern of sample f is plotted. After Rietveld refinement, the QPA gives the phase composition presented in Table 3: Al, LiH, $LiBH_4$, and finally LiCl were identified. No other phases could be indentified despite the presence of a small unexplained peak at $2\theta = 27.45°$. Voigt functions were used to fit the peaks and two different LiCl phases had to be used to fit the LiCl peak shape (see the inset in Figure 6). Indeed, LiCl has two origins: it is an impurity in the purchased $LiAlH_4$, and it is formed during the reduction of $TiCl_3$. The broader peaks were attributed to the LiCl formed during the reduction reaction, assuming that it consists of

TABLE 3: Phases Composition for Sample f (in mol %), Obtained from QPA on the Refined Diffraction Pattern of Figure 6

sample	Al	LiH	$LiBH_4$	LiCl	LiCl (impurity)
f	41 (42.85, 42.85)[a]	43 (41.88, 42.85.)	14 (14.28, 13.42)	0.9 (0.85, 0.85)	0.8

[a] The first numbers in the parentheses correspond to the theoretical values calculated from eq 6, the second from eq 7.

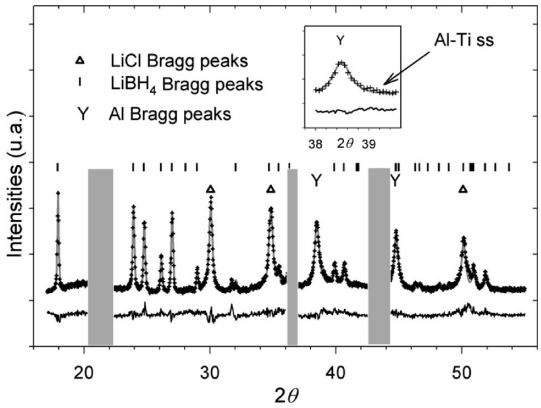

Figure 7. BRUKER PXD pattern of sample h. The dots are the experimental points, the line is the refined pattern, and the line under the pattern is the difference between the experimental and the refined pattern. The inset, top right corner, is an enlargement of the Al (111) reflection showing the Al−Ti solid solution (ss) tail on the peak. The gray rectangles are the regions excluded from the refinement (peaks due to the sample holder).

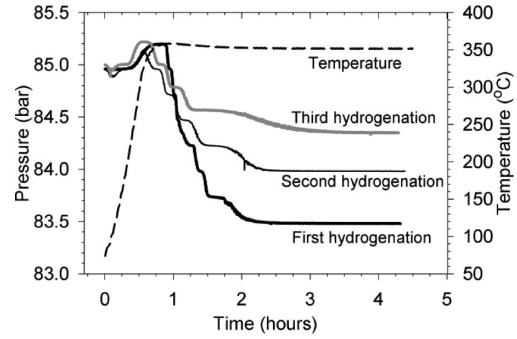

Figure 8. Evolution of the pressure and temperature versus time during the hydrogenation cycles of sample f.

smaller crystallites than the LiCl considered as an impurity. The lithium in LiCl may come from LiH and/or $LiBH_4$ via either of the following two reactions:

$$LiBH_4 + xLiH + xAl + yTiCl_3 \xrightarrow{BM} LiBH_4 + (x - 3y)LiH + 3yLiCl + xAl + yTi + \frac{3y}{2}H_2 \quad (6)$$

$$LiBH_4 + xLiH + xAl + yTiCl_3 \xrightarrow{BM} (1 - 3y)LiBH_4 + 3yB + xLiH + 3yLiCl + xAl + yTi + 6yH_2 \quad (7)$$

Both reactions give similar compositions. It was not possible to determine which one dominates from quantitative phase analysis.

3.2.3. $LiBH_4$ Mixed with LiH + Al. From XRD measurements (not shown here) no phases other than Al, LiH, and $LiBH_4$ were found in sample j. No chemical reactions occur, and the milling produces a physical mixture of the three phases. By applying the Scherrer equation on the aluminum peaks, a mean aluminum crystallite size of ~66 nm was obtained. This result is reliable. The diffraction pattern is of good quality, there are not too many phases in the sample, the aluminum is pure (no Ti), and its scattering power is much larger than the one of the other compounds present. The Al peaks are well resolved and the Al peak width, apart from the instrumental contribution, can be related to the mean grain size. Al grain sizes in the range from 100 to 150 nm where obtained for the other samples from the X-ray peak widths and a 100 nm grain was observed in the TEM images for sample d.

3.2.4. $LiBH_4$ Mixed with 10 mol % (LiCl + 3Al + Ti). A PXD pattern of sample h is shown in Figure 7. No phases other than Al, LiCl, and $LiBH_4$ were identified. There is a tail on the right side of the aluminum peaks (see inset Figure 7), which has been identified, for the sodium Alanate system mixed with $TiCl_3$, as a solid solution (ss) of Ti and Al.[18,20] This solid solution results from the milling of $LiAlH_4$ and $TiCl_3$. Here, one can conclude that no significant reaction seems to occur during the milling of $LiBH_4$ with LiCl + 3Al + Ti.

3.3. Reversibility and Cycling. The samples were investigated for reversibility under ~85 bar of H_2 at 350 °C; 85 bar was the maximum pressure available on the Sievert's setup. Three samples were found to be reversible under these relatively moderate conditions: samples d ($LiBH_4$ + 3$LiAlH_4$ + 4 mol % $TiCl_3$), f ($LiBH_4$ + 3(LiH + Al) + 2 mol % $TiCl_3$), and j ($LiBH_4$ + 3(LiH + Al)), the other samples showed no or only very poor reversibility. The low reversibility of sample b, h, and d is believed to be due to the large amount of $LiBH_4$ in their composition. Indeed, $LiBH_4$ melts upon heating to 350 °C, and release hydrogen. The gas, bubbling in the melt, may carry some of the liquid or vapor phase out of the reactor. This is confirmed by the presence of metallic deposits on the outer wall of the reactor after cooling. In the case of the other samples, the presence of a large proportion of solid phases may prevent this evaporation.

Figure 8 displays the evolution of pressure and temperature versus time during the hydrogenation cycles of sample f. The set temperature, 350 °C, is reached in 1 h, and total hydrogenation is achieved within 1−2 h. The observed difference between the three pressure drops in Figure 8 comes mainly from the loss of reversible storage capacity, the difference attributed to the removal of powder for PXD measurements between each cycle (0.5 mg) accounting for less than 0.5 bar. The three samples, d, f, and j, show approximately the same time to recharge.

In Figure 9, TDS curves for the first to fourth dehydrogenation cycles of samples f and j are shown. The reversible H_2 weight capacity decreases for both samples during cycling. It decreases from 2.70 (first dehydrogenation) to 1.90 wt % (fourth dehydrogenation) for sample f and from 2.60 to 1.45 wt % for sample j. Any H_2 wt % larger than 2.4 is an indication that LiH is also decomposed during the TDS. Nevertheless, no phases which may form from Al, Li, and B, like AlLi or LiB where found in the diffraction pattern of the cycled samples. Since the reversible capacity is higher for sample f than for sample j, it can also be stated that Ti and/or the Al−Ti (ss) promotes the reversible decomposition of LiH. For Sample f the hydrogen evolution

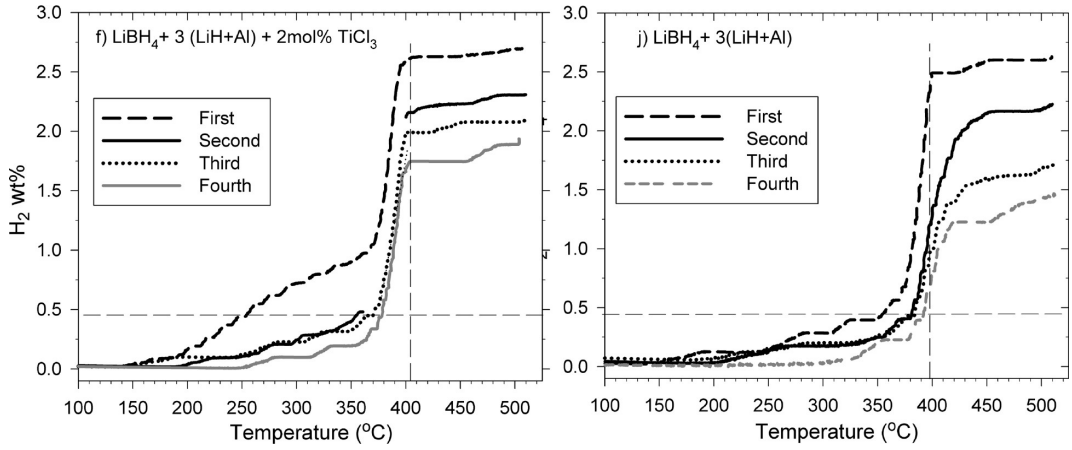

Figure 9. TDS plots of the first to fourth dehydrogenation cycles of samples f and j. The hydrogenations were performed at ~85 bar of H_2, 350 °C.

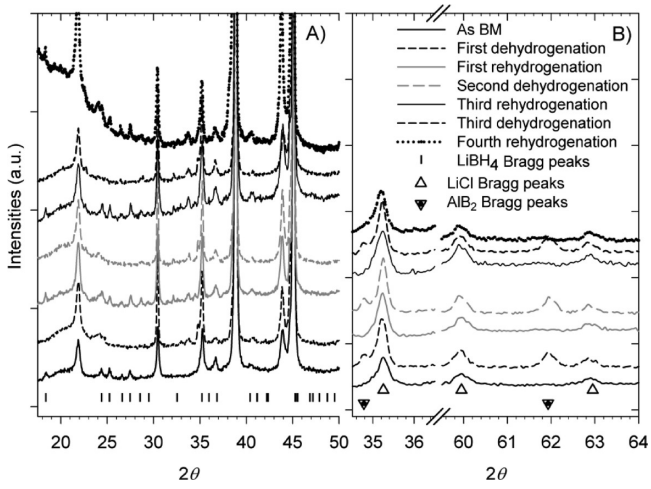

Figure 10. PXD patterns in the hydrogenated/dehydrogenated states of sample f during the three cycles. (A) Wide 2θ range to emphasize $LiBH_4$ cycling. (B) Selected 2θ ranges to emphasize AlB_2 cycling.

ends at around 400 °C and exhibits the same rate over the four cycles. For sample j, the temperature for complete desorption increases from 400 to 440 °C, while the rate decreases. For sample f, PXD patterns were collected after each dehydrogenation and hydrogenation step. They are shown in Figure 10A. $LiBH_4$ present in the pattern of the hydrogenated powder cannot be found in the dehydrogenated powder. Clearly, $LiBH_4$ is the compound involved in the hydrogen cycles.

Aluminum diborides were found to form and vanish during cycling of lithium borane, sample j and f; see the diffraction patterns in Figure 10B for sample f. AlB_2 has a hexagonal symmetry (space group *P6/mmm*). The structural data used herein were taken from ref 26. From the Rietveld refinement, the refined Al and B occupancies result in defects on the aluminum position which correspond to the composition $Al_{0.8}B_2$. The large amount of defects found from the refinement may be due to the limited accuracy of the method; nevertheless, the existence of significant metal deficiency is commonly found in many transition metal diborides.[28] For aluminum diborides, different compositions have been estimated, $Al_{0.93}B_2$ from X-ray emission and absorption spectra,[29] $Al_{0.89}B_2$ from synchrotron powder diffraction data,[30] and $Al_{0.9}B_2$ from X-ray, mass density, and nuclear magnetic resonance measurements.[31] Stoichiometric AlB_2 was found to be unlikely to form.[27,30] From the Al−B phase diagram,[32] the nonstoichiometric hexagonal structure type phase should exist within the range of $0.66 < B/(Al + B) <$ 0.92, in our case the ratio is about 0.71. The exothermic enthalpy of formation of AlB_2 has been calculated to be $\Delta H_f^0 = -7.67$ kJ/mol and its peritectic decomposition will occur at around 972 C°.[32]

The reversible behavior of the $LiBH_4$/Al system seems then to follow the reaction:

$$2LiBH_4 + Al \leftrightarrow 2LiH + AlB_2 + 3H_2 \qquad (8)$$

The loss in the reversible capacity is not well understood and could originate from several effects. At temperatures below 300 °C, formation of B_2H_6 can be expected and cause the loss in the reversible capacity. At temperatures above 300 °C, B_2H_6 is no longer stable. Ming Au et al.[33] found trace amounts of BH_3 and H_2O in the mass spectral analysis of the gas stream from the decomposition of commercial $LiBH_4$. They used the same product as the one used herein. In ref 34, it was found that almost all hydrogen desorption events were accompanied by diborane. Its formation starts at around 170 °C. $TiCl_3$ and $LaCl_3$, used as additives, were found to reduce its formation at temperatures above 350 °C. It is also possible that some boron not participating in the formation of AlB_2 segregates as amorphous clusters, as has been shown in ref 35. Added to this, some well-defined peaks, but with very weak intensity, arose in the diffraction patterns of samples f and j. These peaks, present in the dehydrogenated and hydrogenated states, have not been identified and could belong to either a $Li_2B_xH_x$-type species or boron phase. The boron once trapped in this phase will not then participate in the cycle, resulting in a decrease of the reversible capacity. This latter point has to be clarified.

4. Discussion

From a careful examination of the ball-milled samples, it appears that they all contain ≤100 nm Al and/or Al−Ti (ss) crystallites. Basically, $LiBH_4$ remains unchanged during milling, except for a possible limited reaction with $TiCl_3$. When used alone, $TiCl_3$ has a limited effect (sample i), while Al alone is proved to be active, by lowering the temperature of decomposition, enabling high desorption rate and the reversibility at moderate conditions (sample j). The best results are obtained when both metals are added with the formation of the Al−Ti (ss) (samples b, c, d, and h). The Al−Ti (ss) allows a slow hydrogen release at low temperature and the conservation of kinetic during the cycles. As suggested for $NaAlH_4$ it most probably facilitates hydrogen dissociation and recombination of H_2 molecules

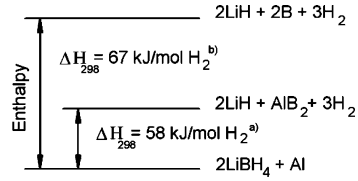

Figure 11. Enthalpy diagram for the $LiBH_4$/Al system. Value a from ref 47; b) from ref 48.

at the hydride surface[24,35] and/or increased mobility of the species involved in the hydrogenation/dehydrogenation.[36−38]

Under ambient conditions, $LiBH_4$ crystallizes with an orthorhombic structure (space group *Pnma*). The tetrahedral anion $[BH_4]^-$ is surrounded by four Li^+ cations each of which is surrounded by four $[BH_4]^-$ ions in a tetrahedral configuration.[21] The hydroboride anion is bonded to the metal atom by bridging hydrogen atoms.

The destabilization of $LiBH_4$ can be achieved by the substitution of Li atoms by cations (M) inducing a charge transfer to $[BH_4]^-$. When $LiBH_4$ donates one electron, the decrease in the hydrogen desorption energy barrier has been calculated[39] and matches with the one observed experimentally.[13] For a complete substitution of Li by M, it has been found both theoretically and experimentally that a correlation exists between the Pauling electronegativity of the cation (M) and the thermodynamical stability of the borohydride.[39,40] This correlation does not apply when there is no or only partial substitution. Indeed, Au et al.[41] and Yang et al.[42] have screened a batch of additives, and if one classifies them with respect to their Pauling electronegativities, the sequence obtained does not match with their effectiveness in destabilizing the hydride. Evidences of partial substitution came recently from Mosegaard et al.[43] They found from an in situ X-ray diffraction study that LiCl, formed from the reduction reaction of $TiCl_3$ by $LiBH_4$, is dissolved to some extent in the structure of solid lithium borohydride at temperatures above ~100 °C, giving an example of a chemical substitution in $LiBH_4$. It is also possible to synthesize by wet chemistry ternary metal borohydrides,[44] and recently a computational screening study has been performed to identify which ternary metal borohydrides may form stable alloys with promising decomposition energies.[45]

Another possible way to destabilize the hydride is the formation of a metal−boron alloy during the dehydrogenation as described by Vajo et al., in their viewpoint paper[46] and Siegel et al.[47] The enthalpy of the dehydrogenated state is reduced by the exothermic formation of the alloy. This is the case herein for the samples containing Al. Figure 11 presents the enthalpy diagram when the AlB_2 alloy is formed in the dehydrogenated state. Clearly, its formation reduces the enthalpy change with a difference of 9 kJ/mol of H_2 between the two reactions (with or without the alloy formation). This latter result is examined in ref 19. Discussing the fact that the difference in the enthalpy is rather small and can even be compensated by an entropy decrease at high temperature, the authors propose that the effect of Al/AlB_2 is rather a kinetic effect related to microstructures of the system.

Yang et al.[42] found a clear relation between the diffusivity of the M/MB_2 species, with reference to their melting point and their abilities to decrease the temperature of desorption by lowering the kinetic barriers. Indeed, it makes sense if one considers the long-range diffusion of the species as one of the main kinetic barriers.

Several studies have shown the system $LiBH_4$ + Al to be reversible. The conditions for rehydrogenation (400 °C, 100 bar;[18] 350 °C, 150 bar;[42] 245−350 °C, 70−100 bar;[48] and 500 °C, 30 bar[49]) were slightly harsher than in the present study using oxygen free Al from $LiAlH_4$. It was found that an increase in the amount of aluminum will decrease the temperature for desorption. As in this study, the storage capacity is found to decrease upon cycling,[18,42,48] although nothing is mentioned about this in ref 49. It has been observed for the $LiBH_4$ + MgH_2 system that desorption conducted against a backpressure of a few bars of hydrogen favors the formation of the desired metal boride, MgB_2, over the formation of boron.[50] Yang et al.[42] found a larger storage capacity and a faster rehydrogenation when applying a back pressure of 3 bar during desorption. On the basis of these results, a study on the effect of the application of back-pressure during the dehydrogenation should be conducted and the effect on the formation of B_2H_6 monitored.

5. Conclusions

Modification of $LiBH_4$ with additives such as Al and Ti reduced the hydrogen desorption temperature, so that decomposition started at 200 °C and ended at 400 °C compared to 300 to 480 °C for pure $LiBH_4$. The modified lithium borohydride can desorbed reversibly up to 12−13.5 wt % of hydrogen, 2−2.4 wt % when the whole mass of the system is considered, at the comparatively moderate conditions of 85 bar and 350 °C. The full rehydrogenation is completed within 2 h. The gradual loss of hydrogen storage capacity with cycling could be attributed to B_2H_6 formation at temperatures below 300 °C. Studies should be conducted in order to assess how to avoid the formation of B_2H_6 by, for example, using a back-pressure during dehydrogenation.

The conditions of hydrogenation and dehydrogenation are still too extreme for mobile applications, and the reversible capacity for the whole system is low. Nevertheless, the low temperature for the decomposition to begin is a good indication and gives encouragement for further study on this material.

Acknowledgment. This project was financially supported by Danish National Energy Research Program (EFP) and Nordic Centre of Excellence on Hydrogen Storage Materials.

References and Notes

(1) Züttel, A.; Rentsch, S.; Fischer, P.; Wenger, P.; Sudan, P.; Mauron, Ph.; Emmenegger, Ch. *J. Alloys Compd.* **2003**, *356−357*, 515–520.
(2) Pistorius, C. *Z. Phys. Chem. Neue Folge (Weisbaden)* **1974**, *88*, 253.
(3) Lodziana, Z.; Vegge, T. *Phys. Rev. Lett.* **2004**, *93*, 14–145501.
(4) Lodziana, Z.; Vegge, T. *Phys. Rev. Lett.* **2006**, *97*, 11–119602.
(5) Fedeneva, E. M.; Alpatova, L.; Mikheeva, V. I. *Russ. J. Inorg. Chem.* **1964**, *9*, 826–827.
(6) Stasinevich, D. S.; Egorenko, G. A. *Russ. J. Inorg. Chem.* **1968**, *13*, 341–343.
(7) Laversenne, L.; Bonnetot, B. *Ann. Chim. Sci. Mater.* **2005**, *30*, 495–503.
(8) Nakamori, Y.; Miwa, K.; Ninomiya, A.; Li, H.; Ohba, N.; Towata, S. I.; Züttel, A.; Orimo, S.-I. *Phys. Rev. B* **2006**, *74*, 045126−1−045126−9.
(9) Orimo, S. I.; Nakamori, Y.; Ohba, N.; Miwa, K.; Oaki, M., I.; Towata, S.; Züttel, A. *App. Phy. Lett.* **2006**, *89*, 021920.
(10) Her, J.-H.; Yousufuddin, M.; Zhou, W.; Jalisatgi, S. S.; Kulleck, J. G.; Zan, J. A.; Hwang, S.-J.; Bowman, R. C.; Udovic, T. J. *Inorg. Chem.* **2008**, *47*, 9757–9759.
(11) Hwang, S.-J.; Bowman, R. C.; Reiter, J. W., Jr.; Rijssenbeek, J.; Soloveichik, G. L.; Zhao, J.-C.; Kabbour, H.; Ahn, C. C. *J. Phys. Chem.* **2008**, *112*, 3164–3169.
(12) Muller A., Mathey F., Bensoam J. *Production of Hydrogen*. U.S. Patent 4,193,978, March 18, 1980.
(13) Züttel, A.; Rentsch, S.; Fischer, P.; Wenger, P.; Sudan, P.; Mauron, Ph.; Emmenegger, Ch. *J. Alloys Compd.* **2003**, *356−357*, 515–520.
(14) Vajo, J. J.; Skeith, S. L.; Mertens, F.; The, *J. Phys. Chem. B* **2005**, *109*, 3719–3722.
(15) Orimo, S.; Nakamori, Y.; Kitahara, G.; Miwa, K.; Ohba, N. *J. Alloys Compd.* **2005**, *404−406*, 427–430.

(16) Yu, X. B.; Grant, D. M.; Walker, G. S. *Chem. Comm.* **2006**, 3906–3908.
(17) Cho, Y. W.; Shim, J. H.; Lee, B-.J. *Calphad* **2006**, *30*, 65–69.
(18) xiang-dong kang, X.-D.; Wang, P.; Ma, L.-P.; Cheng, H-. M. *Appl. Phys. A: Mater. Sci. Process.* **2007**, *89*, 963–966.
(19) Friedrichs, O; Kim, J. W.; Remhof, A.; Buchter, F.; Borgschulte, A.; Wallacher, D.; Cho, Y. W.; Fichtner, M.; Oh, K. H.; Züttel, A. *Phys. Chem. Chem. Phys.* **2009**, *11*, 1515–1520.
(20) Hunter B., IUCR Powder DiffractionNewsletter, 1998, 20.
(21) Soulié, J.-Ph.; Renaudin, G.; Cerny, R.; Yvon, K. *J. Alloys Compd.* **2002**, *346*, 200–205.
(22) Garner, W.; Haycok, F. *Proc. R. Soc. London, A* **1952**, *211*, 335–351.
(23) Haiduc, A. G.; Stil, H. A.; Schwarz, M. A.; Paulus, P.; Geerlings, J. J. C. *J. Alloys Compd.* **2005**, *393*, 252–263.
(24) Blanchard, D.; Brinks, H. W.; Hauback, B.; Norby, C. P. *Mater. Sci. Eng., B* **2004**, *108*, 54–59.
(25) Vegge, T. *PCCP* **2006**, *8*, 4853–4861.
(26) Brinks, H. W.; Jensen, C. M.; Srinivasan, S. S.; Hauback, B. C.; Blanchard, D.; Murphy, K. *J. Alloys Compd.* **2004**, *376*, 215.
(27) Burkhardt, U.; Gurin, V.; Haarmann, F.; Borrmann, H.; Schnelle, W.; Yaresko, A.; Grin, Y. *J. Solid State Chem.* **2004**, *177*, 389–394.
(28) Prokhorov, A. M.; Lyakishev, N. P.; Burkhanov, G. S.; Dement'ev, V. A. *Inorg. Mater.* **1996**, *32*, 1195.
(29) Nakamura, J.; Watanabe, M.; Oguchi, T.; Nasubida, S.; Kabasawa, E.; Yamada, N.; Kuroki, K.; Yamazaki, H.; Shin, S.; Umeda, Y.; Minakawa, S.; Kimura, N.; Aoki, H. *J. Phys. Soc. Jpn.* **2002**, *71*, 408–410.
(30) Loa, I.; Kunc, K.; Syassen, K.; Bouvier, P. *Phys. Rev. B* **2002**, *66*, 134101−1134101−8.
(31) Mirkovi'c, D.; Gröbner, J.; Schmid-Fetzer, R.; Fabrichnaya, O.; Lukas, H. L. *J. Alloys Compd.* **2004**, *384*, 168–174.
(32) Massalski T. B., Okamoto H., Subramanian P. R., Kacprzak L. *Binary Phase Diagrams*, 2nd edition. s.l.: ASM International: Materials Park, OH, 1990.
(33) Au, M.; Jurgensen, A. *J. Phy. Chem. B* **2006**, *110*, 7062–7067.
(34) Kostka, J.,; Lohstroh, W.; Fichtner, M.; Hahn, H. *J. Phys. Chem. C* **2007**, *111*, 14026–14029.
(35) Kim, J. W.; Friedrichs, O.; Ahn, J.-P.; Kim, D. H.; Kim, S. C.; Remhof, A.; Chung, H.-S.; Lee, J.; Shim, J.-H.; Cho, Y. W.; Züttel, A.; Oh, K. H. *Scr. Mater.* **2009**, *60*, 1089–1092.
(36) Bellosta von Colbe, J. M.; Schmidt, W.; Feldherhoff, M.; Bogdanovic, B.; Scüth, F. *Angew. Chem., Int. Ed.* **2006**, *45*, 3663–3665.
(37) Lohstroh, W.; Fitchner, M. *Phys. Rev. B* **2007**, *75*, 184106−1184106−6.
(38) Shi, Q.; Voss, J.; Jacobsen, H. S.; Lefmann, K.; Zamponi, M.; Vegge, T. *J. Alloys Compd.* **2007**, *446−447*, 469–473.
(39) Kang, J. K.; Kim, S. Y.; Han, Y. S.; Muller, R. P.; Goddard, W. A. *Appl. Phys. Lett.* **2005**, *87*, 111904−1111904−3.
(40) Au, M.; Jurgensen, A.; Zeigler, K. *J. Phy. Chem. B* **2006**, *110*, 26482–26487.
(41) Au, M.; Spencer, W.; Jurgensen, A.; Zeigler, C. *J. Alloys Compd.* **2008**, *462*, 303–309.
(42) Yang, J.; Sudik, A.; Wolverton, C. *J. Phys. Chem. A* **2007**, *111*, 19134–19140.
(43) Mosegaard, L.; Møller, B.; Jørgensen, J.-E.; Filinchuk, Y.; Cerenius, Y.; Hanson, J. C.; Dimasi, E.; Besenbacher, F.; Jensen, T. R. *J. Phys. Chem. A* **2008**, *112*, 1299–1303.
(44) Nöth, V. D. H. *Angew. Chem.* **1961**, *1961*, 73–11, 371−383.
(45) Hummelshøj, J. S. *J. Chem. Phys.* 2009.
(46) Vajo, J. J.; Olson, G. L. *Scr. Mater* **2007**, *56*, 829–834.
(47) Siegel, D. J.; Wolverton, C.; Ozolins, V. *Phys. Rev. B* **2007**, *76*, 134102−113402−6.
(48) Jin, S.-A.; Shim, J.-H.; Cho, Y. W.; Yi, K.-W.; Zabara, O.; Fichtner, M. *Scr. Mater.* **2008**, *58*, 963–965.
(49) Yu, X. B.; Guo, Z. P.; Liu, H. K. *J. Mater. Res.* 2008.
(50) Vajo, J. J.; Skeith, S. L.; 2005, *J. Phys. Chem. B* **2005**, *109*, 3719–3722.

JP9031892